Treatment of Mine Drainage Using Permeable Reactive Barriers: Column Experiments

K. R. WAYBRANT,[†] C. J. PTACEK,[†,‡] AND D. W. BLOWES*,[†]

Department of Earth Sciences, University of Waterloo, Waterloo, Ontario, N2L 3G1 Canada, and National Water Research Institute, 867 Lakeshore Road, Burlington, Ontario, L7R 4A6 Canada

Permeable reactive barriers designed to enhance bacterial sulfate reduction and metal sulfide precipitation have the potential to prevent acid mine drainage and the associated release of dissolved metals. Two column experiments were conducted using simulated mine-drainage water to assess the performance of organic carbon-based reactive mixtures under controlled groundwater flow conditions. The simulated mine drainage is typical of mine-drainage water that has undergone acid neutralization within aquifers. This water is near neutral in pH and contains elevated concentrations of Fe(II) and SO_4. Minimum rates of SO_4 removal averaged between 500 and 800 mmol d^{-1} m^{-3} over a 14-month period. Iron concentrations decreased from between 300 and 1200 mg/L in the influent to between <0.01 and 220 mg/L in the columns. Concentrations of Zn decreased from 0.6−1.2 mg/L in the input to between 0.01 and 0.15 mg/L in the effluent, and Ni concentrations decreased from between 0.8 and 12.8 mg/L to <0.01 mg/L. The pH increased slightly from typical input values of 5.5−6.0 to effluent values of 6.5−7.0. Alkalinity, generally <50 mg/L (as $CaCO_3$) in the influent, increased to between 300 and 1300 mg/L (as $CaCO_3$) in the effluent from the columns. As a result of decreased Fe(II) concentrations and increased alkalinity, the acid-generating potential of the simulated mine-drainage water was removed, and a net acid-consuming potential was observed in the effluent water.
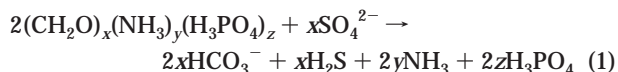
Introduction

The oxidation of sulfide minerals within mine-tailings impoundments results in the generation of low quality water characterized by low pH and high concentrations of dissolved SO_4, Fe(II), and other metals (*1*). As this low pH water migrates through the tailings and underlying aquifers, it undergoes a series of dissolution and precipitation reactions that generally result in acid neutralization (Figure 1; *1*, *2*). The resulting plume water is characterized by near-neutral pH; reduced E_h; and elevated concentrations of dissolved SO_4, Fe(II), and other metals. This groundwater ultimately discharges to surface water flow systems where oxidation of Fe^{2+} to Fe^{3+} and the subsequent precipitation of ferric oxyhydroxides can result in the generation of acidity.

The use of bacterially mediated sulfate reduction in permeable reactive barriers is an alternative technique for the remediation of acid mine drainage (*3−6*). Permeable reactive barriers are installed in the path of migrating mine-drainage water by excavating the aquifer material and replacing it with a permeable reactive material (Figure 1). These barriers are designed to remove dissolved Fe^{2+} and other metals from plumes of flowing tailings-impacted groundwater through enhanced biological sulfate reduction and metal sulfide precipitation (*5−7*).

Under favorable conditions, sulfate-reducing bacteria (SRB) catalyze the oxidation of organic carbon coupled with the reduction of sulfate to sulfide through the following general reaction (*6*, *8*):

$$2(CH_2O)_x(NH_3)_y(H_3PO_4)_z + xSO_4^{2-} \rightarrow$$
$$2xHCO_3^- + xH_2S + 2yNH_3 + 2zH_3PO_4 \quad (1)$$

where $(CH_2O)_x(NH_3)_y(H_3PO_4)_z$ represents organic matter undergoing oxidation and x, y, and z are stoichiometric coefficients. The reduction of SO_4 produces H_2S, releases HCO_3^-, and results in an increase in alkalinity and pH. The reaction also releases ammonia and dissolved phosphate, which is utilized by the bacteria or released into the environment (*9*).

An increase in H_2S concentrations coupled with the low solubility of metal sulfides results in the removal of dissolved metals as metal sulfides:

$$Me^{2+} + S^{2-} \rightarrow MeS \quad (2)$$

where Me^{2+} denotes a divalent metal such as Cd, Fe, Ni, Cu, Co, and Zn; MeS represents an amorphous or poorly crystalline metal sulfide (*10*).

The conditions typically found within a reactive barrier environment are well suited to SRB. Permeable reactive barriers provide dissolved C, N, and P, and the plume water entering the barrier provides high concentrations of SO_4, Fe, and other metals, all of which are necessary for growth and reproduction.

Results of column experiments designed to assess sulfate reduction rates and metal removal capacities of selected reactive mixtures under controlled flow conditions are presented here. These column experiments were conducted under conditions typical of the environment in which permeable reactive barriers would be applied. Laboratory column experiments allow the evaluation of the removal of dissolved metals including Fe, Ni, Zn, and SO_4 under closely controlled flow conditions and allow the direct evaluation of sulfate and metal removal rates.

Methodology

Column Design and Experimental Setup. Two 5 cm diameter, 40 cm long acrylic columns were packed with 5 cm of silica sand and crushed pyrite on the bottom followed by 33.5 cm of reactive mixture and topped with 1.5 cm of silica sand. The bottom and top layers separate the reactive mixture from the influent and effluent ports. The influent and effluent ports were separated from the packing material with a coarse-meshed nylon screen followed by a fine-meshed NYTEX screen to prevent material from being washed out of the columns. Crushed pyrite was added to the bottom layer to consume O_2 and Fe(III) in the influent water. The reactive mixtures consisted of an organic source, a bacterial source, a neutralizing agent, and a nonreactive porous medium (Table 1). The organic carbon source included mixtures of wood chips, sawdust, composted municipal sewage sludge,

* Corresponding author phone: (519)888-4878; fax: (519)746-3882; e-mail: blowes@sciborg.uwaterloo.ca.
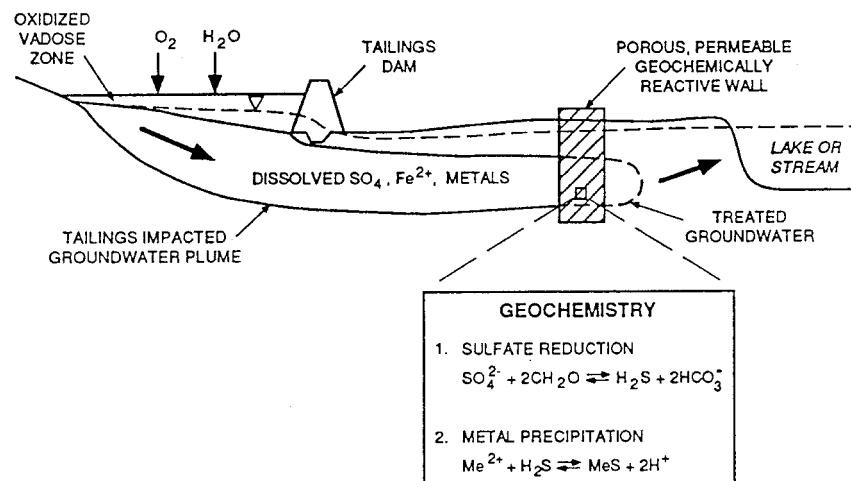† University of Waterloo.
‡ National Water Research Institute.

GEOCHEMISTRY

1. SULFATE REDUCTION

$$SO_4^{2-} + 2CH_2O \rightleftharpoons H_2S + 2HCO_3^-$$

2. METAL PRECIPITATION

$$Me^{2+} + H_2S \rightleftharpoons MeS + 2H^+$$

FIGURE 1. Schematic diagram of permeable reactive barrier at a mine drainage site.

TABLE 1. Composition of Reactive Mixtures Used in Column Experiments[a]

mixture composition	column 1 (dry wt %)	column 2 (dry wt %)
bottom layer (5 cm)		
crushed pyrite	10	10
silica sand	90	90
middle layer (33.5 cm)		
composted leaf mulch	19.5	23
wood chips	8	
sawdust	10.5	22
sewage sludge	10	
creek sediment	43	44
agricultural limestone	2	3
silica sand	7	8
top layer (1.5 cm)		
silica sand	100	100

[a] Flow is from bottom to top.

and leaf compost from a municipal recycling program. Two different reactive mixtures were used: one containing leaf mulch, sawdust, sewage sludge, and wood chips (column 1) and the other containing leaf mulch and sawdust (column 2). These mixtures correspond closely to batch mixtures previously evaluated in bench-scale batch studies (5) and in a full-scale reactive barrier installation (6, 7). The bacterial source was collected from the anaerobic zone of a local creek.

The reactive mixtures were soaked in a $CaCO_3$-saturated solution containing 1000 mg/L SO_4 as $CaSO_4$ and 5% sodium lactate. The $CaCO_3$-saturated water was made by adding $CaCO_3$ in excess to a known volume of double-deionized water and was bubbled with high-purity $CO_2(g)$ for several hours. This solution was left to equilibrate with the atmosphere for several days to weeks before use. The mixtures were packed into the columns wet to prevent aeration of the bacterial source. The $CaSO_4$ and sodium lactate were added to help acclimate the bacteria and promote sulfate-reducing conditions. Columns were covered with aluminum foil to exclude light and prevent growth of photolithotrophic bacteria. Within 30–40 days an active population of SRB was established, as was evident from the production of H_2S gas. The columns were transferred into an anaerobic glovebox. The anaerobicity of the glovebox was monitored regularly using methylene blue anaerobic strip indicators (GasPak).

The same input solution was used for both columns. The initial input solution (feed) contained 1000 mg/L SO_4 as $CaSO_4$, made up using double-deionized water saturated with $CaCO_3$. This input solution was used for the first 4 pore volumes (pv) (feed 0, Table 2), after which simulated mine water was used for the remainder of the study (feeds 1–8, Table 2). The chemical composition of the simulated mine water was based upon observations made at a mine-tailings impoundment (6). New input solutions were prepared every 5–6 weeks. This allowed the input solution to be modified as necessary.

A conservative tracer test was performed on both columns by adding NaBr to the feed 1 input solution and measuring effluent Br^- concentrations over time. The conservative tracer tests were used to determine the effective pore volumes of the saturated columns.

Influent concentrations of Ni and Mn were higher in feed 4 as a result of laboratory error. The concentration of Fe in the input solution was decreased in feed 5 after a minor breakthrough of Fe was observed in both of the columns. This decrease in Fe was accompanied with decreases in concentrations of dissolved SO_4 and metals. After 18.5 pv, NH_4Cl was added as a nutrient to determine if the mixture was nitrogen-limited. The amount of NH_4Cl added to the influent corresponded to 7 mg/L nitrogen. This value was based upon a C:N ratio of 25:1. The carbon content was based upon early DOC measurements in the effluent. The chemical composition and input duration of each input solution are given in Table 2. The simulated mine water was stored in an O_2-free environment to prevent oxidation of Fe^{2+} to Fe^{3+}, thus keeping the pH relatively constant at 5.5–6.5 (Table 2).

A variable speed, multichannel pump (ISMATEC) was used to deliver the influent to each of the columns to yield an average linear velocity of $\cong 10$ m/a. Stainless steel tubing was used between the feed reservoir and the glovebox (i.e., where it was exposed to an oxic environment), and either stainless steel or PharMed tubing was used in anoxic areas. The column effluent solutions were collected in flow-through sample cells within the glovebox, and overflow was directed to waste jugs outside of the glovebox. Flow rates (mL/h) were determined by measuring the overflow.

Sample Collection. Column effluent samples were collected within the glovebox to determine pH, E_h, alkalinity, and concentrations of dissolved Br, Ca, Cd, Cl, Fe, H_2S, K, Mg, Mn, Na, Ni, o-PO_4, SO_4, Zn, dissolved organic carbon (DOC), dissolved inorganic carbon (DIC), $\delta^{34}S$, and volatile fatty acids (acetic acid, propionic acid, butyric acid, and formic acid). Measurements of pH, E_h, and alkalinity were determined immediately after sampling. The pH and E_h were measured on unfiltered samples in sealed cells to minimize O_2 exposure, and a filtered sample was used for measuring alkalinity. Electrode calibration and performance were checked before and after each sample measurement. The

TABLE 2. Duration (Pore Volumes (pv)) and Composition of Input Solution Used in Column Experiments 1 and 2

input soln	duration column 1 (pv)	duration column 2 (pv)	pH	E_h (mV)	alkalinity (mg/L as CaCO₃)	SO₄ (mg/L)	Fe (mg/L)	Zn (mg/L)	Ni (mg/L)	Mn (mg/L)	Na (mg/L)	Ca (mg/L)	K (mg/L)	Mg (mg/L)	Br (mg/L)	Cl (mg/L)
feed 0	0–0.47	0–5.9				1010									0	
feed 1	4.7–7.4	5.9–8.3	6.40	16	147.1	3210	694	0.72	0.94	9.75	46.8	506	27.4	242	26	14.2
feed 2	7.4–9.2	8.3–10.1	5.85	74	54.8	3894	1181	0.95	1.40	12.9	50.0	99	31.7	320	0	4.82
feed 3	9.2–12.0	10.1–12.9	6.41	142	45.0	3455	876	0.58	1.31	12.8	48.8	92	32.3	317	0	5.16
feed 4	12.0–15.5	12.9–16.1	6.46	179	34.0	3660	956	0.97	12.3	19.8	48.8	83	29.2	288		7.71
feed 5	15.5–18.4	16.1–18.7	6.60	2	25.9	2000	444	1.22	2.34	14.1	14.1	205	11.8	121		0.91
feed 6	18.4–21.5	18.7–21.7	6.16	23	11.2	1623	379	0.85	1.60	8.96	8.96	214	7.9	83		15.4
feed 7	21.5–24.9	21.7–24.8	6.61	307	27.8	1353	334	0.57	3.36	8.62	8.62	220	7.2	77		17.6
feed 8	24.9–27.7	24.8–27.5	6.43	180	23.8	1400	316									14.4

pH electrode (Orion Ross Sure-Flow Combination pH 81-65) was calibrated using standard 4.0 and 7.0 buffers (referenced to NIST SRM), and the E_h electrode (Orion 96-78) was checked using Zobell's solution (11). The alkalinity was determined using standardized H_2SO_4 and a Hach digital titrator. Samples were filtered through a 0.45-μm cellulose acetate filter paper, and both acidified and nonacidified samples were collected and stored at 5 °C until analyses were completed within 60 days unless otherwise specified. Analytical procedures were the same as those described previously for batch tests conducted using similar materials (5).

Mineralogical Characterization. After 30 months of flow through column 2, a subsample of the reactive material was removed from column 2 and examined to determine the nature of the reaction products. Column material from the influent end was examined using a Hitachi S-4500 field emission secondary electron microscope. EDX analyses were obtained using a Noran Instruments light element detector attached to an ISI DS-130 scanning electron microscope.

Results and Discussion

Conservative Tracer Test and Modeled Velocity and Dispersion Coefficient. A pulse style conservative tracer test was performed to determine the effective pore volume of each column under saturated conditions. Calculated effective pore volumes for columns 1 (leaf mulch, sawdust, sewage sludge, and wood chips) and 2 (leaf mulch and sawdust) were 420 and 480 mL, respectively. The transport model CXTFIT (12) was used to determine the velocity and dispersion coefficient in each column. Fitted velocity estimates for columns 1 and 2 were 9.5 ($\pm$ 0.01) and 9.7 ($\pm$ 0.02) m/yr, respectively; calculated dispersion coefficients were 0.18 ($\pm$ 2.0×10^{-3}) m²/yr for column 1 and 0.13 ($\pm$ 2.0×10^{-3}) m²/yr for column 2.

Measured Sulfate Reduction Rates and Metal Removal Capacity. The long-term effectiveness of permeable reactive barriers depends on maintaining the conditions conducive to biological sulfate reduction. Several factors may affect the rate of sulfate reduction, among these the reactivity of the carbon source and the residence time are perhaps the most important. Sulfate reduction rates are used to indicate the reactivity of the mixture. Sulfate reduction rates for the column experiments were approximated by sulfate-removal rates (13), which were determined by subtracting the measured effluent SO₄ concentrations subject to conservative transport and SO₄ reduction from modeled effluent SO₄ concentrations considering conservative transport only and dividing this quantity by a time or volume interval. Modeling the effluent concentration considering dispersion and displacement allowed a more accurate calculation of sulfate removal as the SO₄ concentration of the input solution varied over time. CXTFIT was used to model effluent SO₄ concentrations using the fitted velocity and dispersion values previously obtained.

The geochemical speciation mass-transfer model MINTEQA2 (14) was used to indicate chemical equilibrium
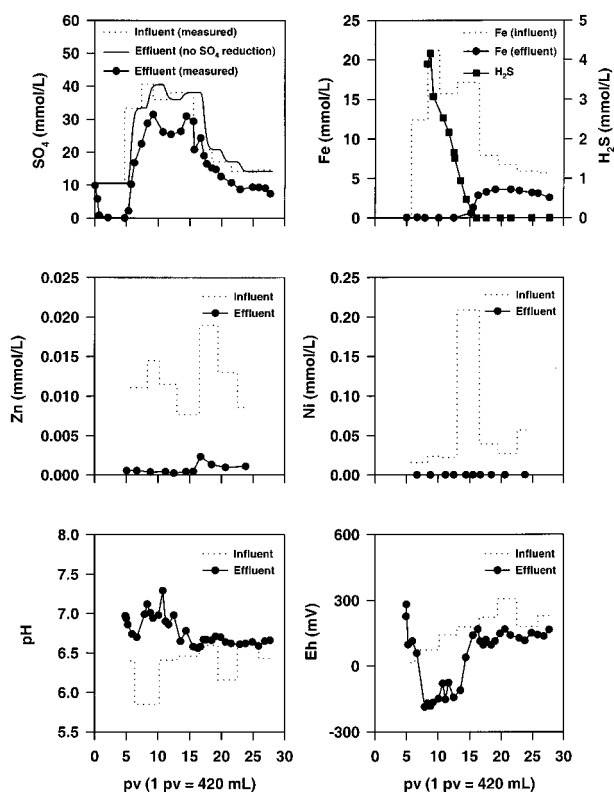

FIGURE 2. Aqueous concentrations of SO₄, Fe, Zn, and Ni and values of pH and E_h for the influent and effluent for column 1. Influent concentrations have been displaced by 1 pore volume.

reactions potentially controlling the concentrations of dissolved constituents in the effluent water. The original database was modified to make it consistent with the WATEQ4F database (15). Saturation indices (SI), where SI = log(IAP/K_{sp}), for various mineral phases were calculated for the column effluent solutions assuming that all measured alkalinity was present as carbonate species, pH was entered and fixed as the measured value, and E_h was calculated based upon measured concentrations of the redox couple HS⁻/ SO₄²⁻. The assumption that all measured alkalinity was carbonate was based upon earlier observations in batch experiments (5), which showed that DOC had a negligible affect on calculated SI values at the observed DOC concentrations. Concentrations of Ni were entered as the detection limit (0.006 mg/L) because measured concentrations in the effluent were often at or below detection in both columns.

Column experiments were run for over 14 months. During this time >27 pv (11–13 L) of simulated mine water was pumped through each column. The input solution varied over time with SO₄ input concentrations ranging from 1000 to 4000 mg/L (10–40 mmol/L) (Table 2); consequently, SO₄ effluent concentrations also varied over time. Monitoring of
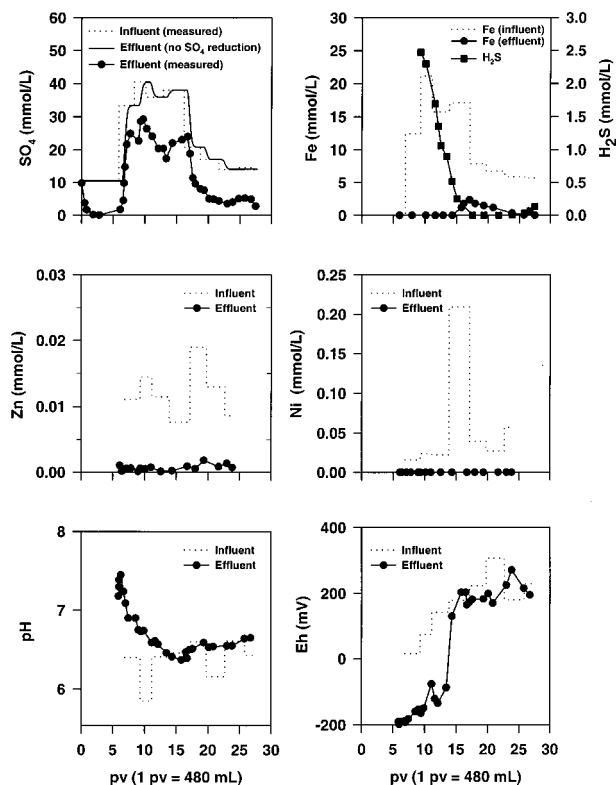
FIGURE 3. Aqueous concentrations of SO_4, Fe, Zn, and Ni and values of pH and E_h for the influent and effluent for column 2. Influent concentrations have been displaced by 1 pore volume.

TABLE 3. Calculated Sulfate Reduction Rates for Column 1[a]

input solution	pore vol (pv)	sulfate reduction rate (mg of SO_4 L^{-1} pv^{-1})	sulfate reduction rate (mmol of SO_4 d^{-1} m^{-3})
feed 0, no metals	0.0−4.7	862	441
feed 1, metals added	4.7−7.4	1089	768
feed 2	7.4−9.2	842	566
feed 3	9.2−12.0	1116	775
feed 4	12.0−15.5	749	549
feed 5	15.5−18.4	924	700
feed 6, $NHCl_4$ added	18.4−21.5	638	455
feed 7	21.5−24.9	592	429
feed 8	24.9−27.7	498	365
average	0.0−27.70	812	510

[a] Sulfate reduction rates were calculated by subtracting measured effluent sulfate concentrations subject to dispersion, displacement, and bacterial sulfate reduction from modeled sulfate concentrations considering dispersion and displacement only.

TABLE 4. Calculated Sulfate Reduction Rates for Column 2[a]

input solution	pore vol (pv)	sulfate reduction rate (mg of SO_4 L^{-1} pv^{-1})	sulfate reduction rate (mmol of SO_4 d^{-1} m^{-3})
feed 0, no metals	0.0−5.9	863	548
feed 1, metals added	5.9−8.3	792	512
feed 2	8.3−10.1	965	631
feed 3	10.1−12.9	1379	934
feed 4	12.9−16.1	1786	1209
feed 5	16.1−18.7	1161	789
feed 6, $NHCl_4$ added	18.7−21.7	1204	820
feed 7	21.7−24.8	1156	788
feed 8	24.8−27.5	898	613
average	0.0−27.5	1134	761

[a] Sulfate reduction rates were calculated by subtracting measured effluent sulfate concentrations subject to dispersion, displacement, and bacterial sulfate reduction from modeled sulfate concentrations considering dispersion and displacement only.

effluent SO_4, H_2S, pH, E_h, and alkalinity (Figures 2 and 3) indicated that sulfate-reducing conditions were maintained throughout the experiments.

The initial input solution contained 1000 mg/L SO_4 as $CaSO_4$ and did not contain dissolved metals. This input solution was used for the first 4.7 and 5.9 pv in columns 1 and 2, respectively (Table 2). Sulfate reduction reactions during this period resulted in the removal of SO_4 from an input concentration of 1000 mg/L (10 mmol/L) to <20 mg/L (0.21 mmol/L) in both columns (Figures 2 and 3). The almost complete (98%) removal of SO_4 suggested that the initial SO_4 concentration limited the extent of SO_4 reduction. As a result of low SO_4 concentrations in the effluent and the lack of dissolved metals in the influent, it was not possible to accurately estimate the potential maximum rate of SO_4 reduction or the metal removal capacity. To quantitatively estimate the rate of SO_4 reduction and to determine the metal removal capacity within the columns, the input solution was modified to contain approximately 3000−4000 mg/L (30−40 mmol/L) SO_4; 700−1200 mg/L (12−20 mmol/L) Fe; and low concentrations of Zn, Ni, Mn, and other dissolved metals (Table 2). This input solution was used between pv 5 and 16, after which the SO_4 and Fe concentrations were lowered (Table 2).

Subtracting the measured effluent SO_4 concentrations subject to conservative transport and sulfate reduction from the modeled effluent SO_4 concentrations subject to conservative transport only (i.e., dispersion and displacement) for this period (5−16 pv, Figures 2 and 3) indicates a continued removal of ≅1000 mg/L SO_4 (700 mmol d^{-1} m^{-3}) in both columns. Calculated sulfate-removal rates for column 1 (leaf mulch, sawdust, sewage sludge, and wood chips) decreased after 18 pv from ≅900 to 500 mg/L SO_4 (700−400 mmol d^{-1} m^{-3}) and for column 2 remained relatively constant (leaf mulch and sawdust) at ≅1000 mg/L SO_4 (700 mmol d^{-1} m^{-3}) for the duration of the study. The more extensive sulfate

removal at the early part of the experiment may be due to a greater abundance of labile organic carbon, both as carbon present in the sodium lactate added to the column material and as the most labile fraction of the solid organic carbon material. The subsequent decline in sulfate reduction may suggest a depletion of the most labile organic carbon forms. The calculated sulfate reduction rates ranged between 400 and 1200 mmol d^{-1} m^{-3} with an average of between 500 and 750 mmol d^{-1} m^{-3} (Tables 3 and 4). These sulfate reduction rates are higher than previously reported rates of between 0.2 and 600 mmol d^{-1} m^{-3} (*16−18*). These previous studies had shorter residence times and lower input pH values as compared to the column studies presented here. The sulfate reduction rates observed in these experiments, however, are similar to those observed in a field-scale permeable reactive barrier system (*6, 10*).

The reduction of SO_4 was accompanied by a decrease in the effluent water E_h and an increase in pH, alkalinity, and H_2S concentrations (Figures 2 and 3). In systems characterized by high rates of SO_4 reduction, the pH is usually buffered to between 6 and 7 (*6, 19*). A slight increase in the pH of the effluent water was observed from typical input values of 5.5− 6.5 to typical effluent values in both columns of 6.5−7.0 (Figures 2 and 3). This pH increase is attributed to bicarbonate buffering as a result of the generation of bicarbonate through sulfate reduction reactions (eq 1) and is supported by increases in alkalinity (Figures 4 and 5).

The alkalinity increased from <50 mg/L (0.5 mmol/L) (as $CaCO_3$) in the influent to between 900 mg/L (9 mmol/L) and
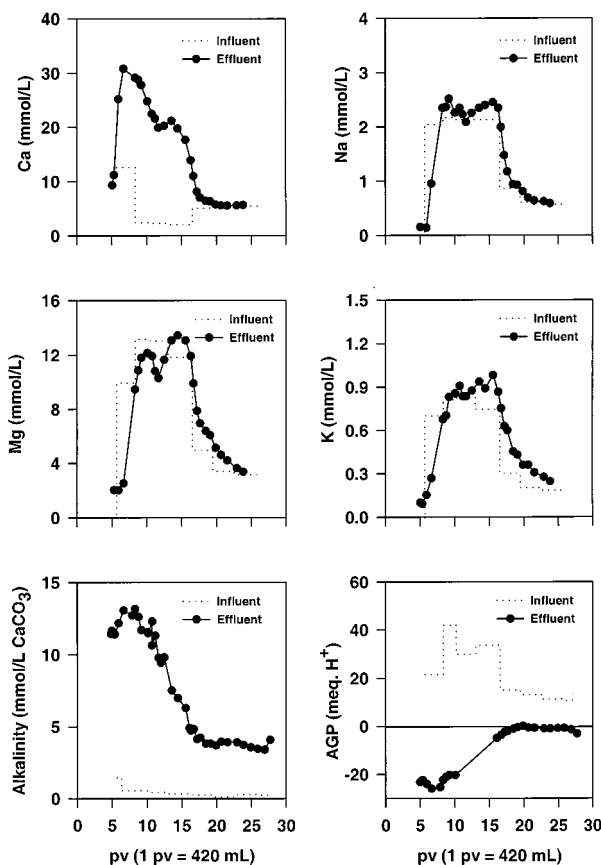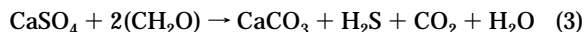
FIGURE 4. Aqueous concentrations of Ca, Mg, Na, K, alkalinity, and calculated acid generating potential (AGP) for the influent and effluent for column 1. Influent concentrations have been displaced by 1 pore volume.
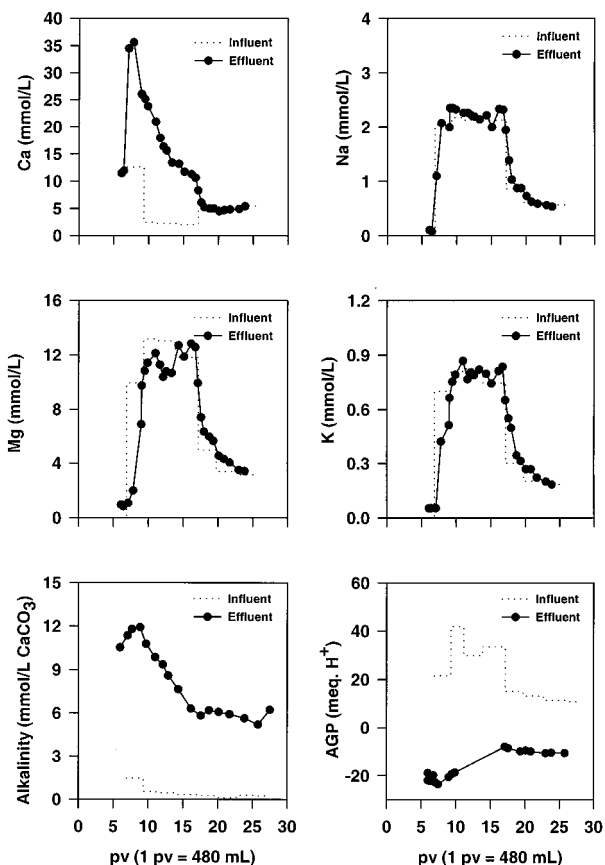

FIGURE 5. Aqueous concentrations of Ca, Mg, Na, K, alkalinity, and calculated acid generating potential (AGP) for the influent and effluent for column 2. Influent concentrations have been displaced by 1 pore volume.
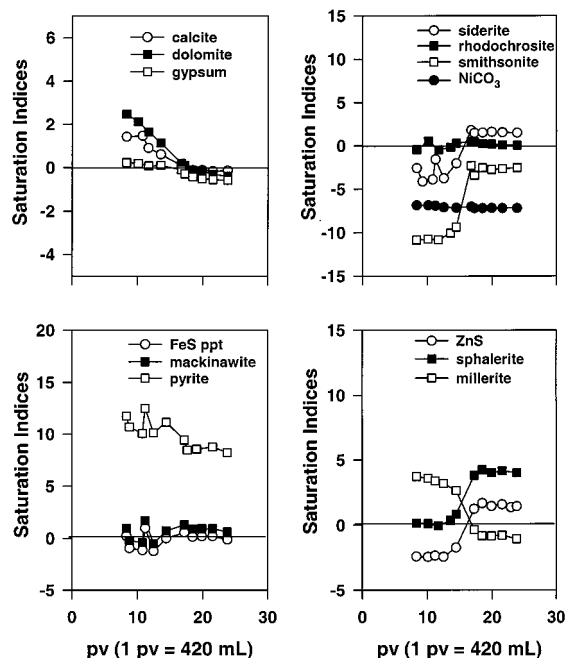
1100 mg/L (11 mmo/L) (as $CaCO_3$) in the effluent initially and then slowly began dropping after 10 pv to between 300 and 600 mg/L (3 and 6 mmol/L) (as $CaCO_3$). The high initial alkalinity values suggest that the rate of sulfate reduction in the early part of the experiment was underestimated or is a result of alkalinity released through other bacterially mediated reactions such as methanogenesis. Calculated sulfate reduction rates were based upon SO_4 concentrations in the influent. The dissolution of gypsum, which was added to the columns as they were set up, was not accounted for in the calculation of sulfate reduction rates. Calculated SI values for the first 15 pv indicate that the effluent water was saturated with respect to gypsum but became undersaturated over time, suggesting depletion of the initial mass of gypsum (Figures 6 and 7). Geochemical analyses of Ca showed an initial increase in Ca from an average input concentration of 200 mg/L (5 mmol/L) to an effluent concentration between 1000 and 1500 mg/L (25 and 37 mmol/L) followed by a gradual decrease in concentrations over time until effluent and influent concentrations were approximately the same (Figures 4 and 5). The initial high Ca concentrations may be attributed to gypsum dissolution, followed by calcite precipitation. Spiro and Aizenshtat (20) hypothesized that high rates of sulfate reduction may lead to the precipitation of calcite through the reaction

$$CaSO_4 + 2(CH_2O) \rightarrow CaCO_3 + H_2S + CO_2 + H_2O \quad (3)$$

Decreasing Ca concentrations, decreasing SI values for gypsum, and positive or near-zero SI values for calcite observed in the experimental results are consistent with eq 3 (Figures 4−7). Effluent concentrations of other major ions

(Mg, Na, and K) followed influent concentrations closely (Figures 4 and 5).

Dissolved sulfide is produced through sulfate reduction reactions (eq 1). Concentrations of H_2S increased from nondetectable concentrations in the influent to values

FIGURE 6. Saturation indices for selected carbonate, sulfate, and sulfide mineral phases for effluent samples from column 1.
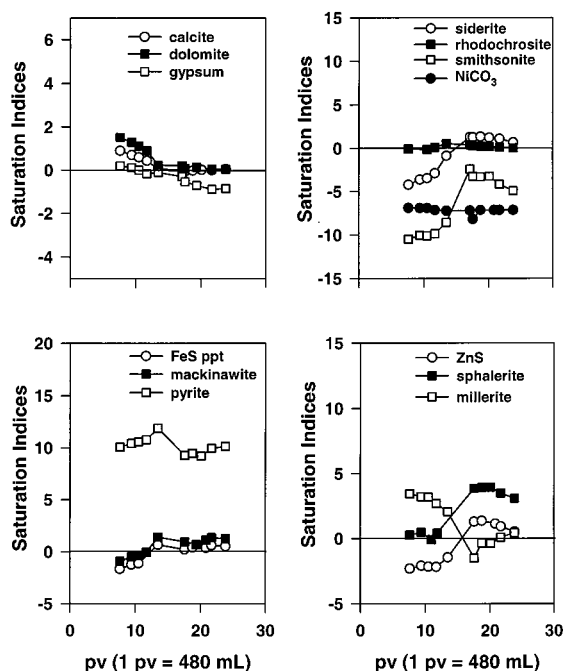
FIGURE 7. Saturation indices for selected carbonate, sulfate, and sulfide mineral phases for effluent samples from column 2.

measured as high as 140 mg/L (4.2 mmol/L) in the effluent (Figures 2 and 3). The observed increases in H_2S were accompanied by decreases in concentrations of dissolved metals in the effluent water (Figures 2 and 3). The most notable were decreases in Fe, which decreased from an influent concentration of between 700 and 1200 mg/L to <0.1 mg/L (12.5 and 21.5 mmol/L to <0.002 mmol/L) (Figures 2 and 3). Concentrations of Zn decreased from 1.0 to <0.15 mg/L (0.015 to <0.002 mmol/L), and Ni decreased from 1.5 to <0.01 mg/L (0.025 to 0.0002 mmol/L) (Figures 2 and 3).

Breakthrough of Fe occurred in both columns 9 pv after the influent Fe and SO_4 concentrations were increased (14 and 15 pv in columns 1 and 2, respectively), coinciding with removal of between 2900 and 3600 mg of Fe. After ≅16 pv, concentrations of SO_4 and Fe in the input solution were lowered by ≅50%.

Effluent H_2S concentrations showed breakthrough of Fe coincided with the almost complete removal of H_2S (Figures 2 and 3). This suggests that the breakthrough represented the amount of dissolved Fe in excess of the amount of H_2S produced and subsequently utilized in the precipitation of metal sulfides during the reduction of 500−1000 mg/L SO_4. Effluent concentrations of Zn and Ni remained low throughout the experiment. The high concentrations of H_2S observed at pv 8 and 9 are attributed to a buildup of H_2S resulting from the absence of Fe and other metals from early input solutions.
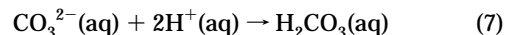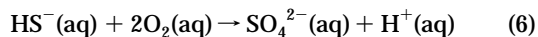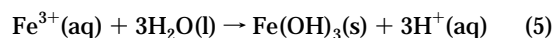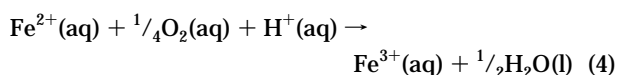
Stoichiometric calculations based upon eq 1 indicate that the reduction of between 500 and 1000 mg/L (5 and 10 mmol/L) SO_4 produces 180−350 mg/L (5 and 10 mmol/L) H_2S. Observations from a field-scale reactive barrier at the Nickel Rim site in Ontario suggest that the most abundant iron sulfide precipitate is mackinawite with an approximate stoichiometry for Fe:S of 1.1 (*10*). If all the H_2S produced was utilized in the precipitation of Fe as FeS (eq 2), then 300−600 mg/L of Fe would be removed from solution. Precipitation of all of the influent Fe, Zn, and Ni as FeS, ZnS, and NiS (using the chemistry of feed 7, Table 2), 230 mg/L or 6.8 mmol of H_2S is required. This amount corresponds to the reduction of 650 mg/L of SO_4. The calculated sulfate reduction rate corresponding to this input solution (Tables 3 and 4) exceeds this value in column 2 (leaf mulch and sawdust) but not in column 1 (leaf mulch, sawdust, sewage sludge, and

wood chips). Consistent with these calculations, effluent from column 2 showed complete removal of Fe, Zn, and Ni and elevated concentrations of H_2S; conversely, effluent from column 1 containing measurable concentrations of Fe and H_2S was not detected or was just above detection (0.01 mg/L detection limit).

The water chemistry data suggest that the primary mechanism for metal removal is through the precipitation of sparingly soluble metal sulfides, and the amount removed is controlled by the H_2S concentration, which is in turn dependent upon the sulfate reduction rate. Geochemical calculations indicate that the effluent water in both columns approached or attained saturation with respect to the mineral phases rhodochrosite ($MnCO_3$), mackinawite ($FeS_{0.9}$), and FeS. These calculations suggest that the carbonate phase, rhodochrosite, or a less crystalline precursor controlled the concentration of Mn and that the sulfide phases, mackinawite and FeS, controlled the concentration of Fe. For the first 14 pv, the SI values for siderite ($FeCO_3$) were negative, suggesting a tendency for $FeCO_3$ to dissolve (Figures 6 and 7). The initial negative SI values for $FeCO_3$ suggest that SO_4 reduction and precipitation of iron sulfide phases was the mechanism resulting in Fe removal. After 14 pv, the effluent approaches saturation with respect to $FeCO_3$ suggesting that the precipitation of both the sulfide phases, FeS and mackinawite, and the precipitation of the carbonate phase, siderite, may affect the concentration of Fe (Figures 6 and 7). Supersaturation with respect to siderite has also been observed in a field-scale permeable reactive barrier system (*6*).

Negative SI values for smithsonite ($ZnCO_3$), positive SI values for amorphous ZnS and sphalerite (ZnS), and low concentrations of Zn in column effluent water samples indicate that Zn concentrations may be controlled by the solubility of a zinc sulfide phase (Figures 2, 3, 6, and 7).

The acid-generating potential (AGP) is a measure of the potential for water to produce acidity. The AGP is calculated by subtracting the acid-producing potential (APP) from the acid-consuming potential (ACP). The APP is a measure of the potential amount of acidity released through the oxidation of Fe^{2+} to $Fe(OH)_3$ (eqs 4 and 5, shown below) and the oxidation of HS^- to produce acidity (eq 6), and the ACP is a measure of the potential to consume acidity through alkalinity represented here as the formation of $H_2CO_3(aq)$ from protonation of $CO_3^{2-}(aq)$ (eq 7):

$$Fe^{2+}(aq) + {}^1/_4O_2(aq) + H^+(aq) \rightarrow$$
$$Fe^{3+}(aq) + {}^1/_2H_2O(l) \quad (4)$$

$$Fe^{3+}(aq) + 3H_2O(l) \rightarrow Fe(OH)_3(s) + 3H^+(aq) \quad (5)$$

$$HS^-(aq) + 2O_2(aq) \rightarrow SO_4^{2-}(aq) + H^+(aq) \quad (6)$$

$$CO_3^{2-}(aq) + 2H^+(aq) \rightarrow H_2CO_3(aq) \quad (7)$$

A positive AGP value indicates a potential to generate acidity, and a negative AGP indicates an acid-neutralizing capacity. Given the close relationship between sulfate reduction reactions and AGP, i.e., the generation of alkalinity (eq 1) and the precipitation of Fe^{2+} as metal sulfides (eq 2), it follows that sufficient rates of sulfate reduction will lead to a decrease in AGP. The AGP of the column influent versus that of the column effluent are shown in Figures 4 and 5. The decrease in AGP from a net APP in the input to a net ACP in the effluent is a direct consequence of the removal of Fe^{2+}, a potential acid-producing metal, and the generation of alkalinity.

The observed decrease in SO_4 and dissolved metals concentrations and the increase in alkalinity and H_2S concentrations are attributed to bacterially mediated sulfate reduction. The predominant isotopes of sulfur in natural

TABLE 5. Sulfur Isotopic Data for Column 1, Column 2, and Input Solutions[a]

sample	SO$_4$ (mg/L)	δ^{34}S (‰ CDT)	f [b]	ϵ [b]
feed 2	3118	1.7	1.0	0.0
column 1	2205	13.8	0.7	−35.3
column 2	2140	16.0	0.7	−38.5
feed 3	3280	2.0	1.0	0.0
column 1	2700	10.2	0.8	−33.0
column 2	2060	20.0	0.6	−38.7
feed 4	3660	1.7	1.0	0.0
column 1	2820	9.0	0.8	−28.0
column 2	2160	20.4	0.6	−35.5
feed 7	1440	4.8	1.0	0.0
column 1	907	25.1	0.6	−43.8
column 2	484	55.1	0.3	−46.1

[a] Calculated enrichment factors (ϵ) show an enrichment of ^{34}S in the column effluent SO$_4$. [b] $f = c_s/c_m$ = residual fraction and $\epsilon = (\delta_s - \delta_m)/\text{Inf}$ = enrichment factor where c_s = residual concentration of sulfate, c_m = initial concentration of sulfate, δ_m = initial value of ^{34}S, and δ_s = residual value of ^{34}S.

systems are ^{32}S and ^{34}S. The relative abundance of these two isotopes is described by their isotopic ratio, which for sulfur is defined as

$$\delta^{34}\text{S}_{\text{sample}} = \frac{m(^{34}\text{S}/^{32}\text{S})_{\text{sample}} - m(^{34}\text{S}/^{32}\text{S})_{\text{reference}}}{m(^{34}\text{S}/^{32}\text{S})_{\text{reference}}} \quad (8)$$

During sulfate reduction, bacteria reduce the lighter ^{32}S isotope in preference to ^{34}S in metabolic functions. As bacterially mediated sulfate reduction proceeds, the lighter ^{32}S isotope predominates in the reduced sulfide and the heavier ^{34}S isotope accumulates in the residual sulfate (21). The extent of ^{34}S enrichment in the residual sulfate is indicated by the residual fractionation factor (f). Determination of the δ^{34}S and calculation of the residual fractionation factor of ^{34}S in SO$_4$ in the effluent water shows an enrichment of δ^{34}S of between −28‰ and −46‰ as SO$_4$ concentrations decreased (Table 5). These values are within the range (−15.5‰ to −60‰) observed in active biological systems (22). Furthermore, the enrichment of ^{34}S increased as the fractionation factor decreased, which also would be expected of SO$_4$ removal by bacterially mediated sulfate reduction (22). Under surficial conditions, abiotic contributions to isotopic fractionation of sulfate are expected to be insignificant. The ^{34}S enrichment observed in the column effluent water indicates that the sulfate removal observed can be attributed to bacterially mediated sulfate reduction.

Mineralogical study of the reactive material following 30 months of column operation was used to identify the reaction products. Small (2−10 μm) spheres were observed on the surfaces of wood particles within the reactive mixture (Figure 8). Energy-dispersion X-ray analysis indicated that these spheres are composed primarily of Fe and S with minor amounts of Ca, Si, Mg, and O. These spheres are interpreted to be precipitates of ferrous monosulfide or mackinawite. Mackinawite and amorphous FeS were identified in samples collected from a full-scale reactive barrier near Sudbury, Ontario (10).

Possible Limitations to the Rate of Sulfate Reduction. It was anticipated that the removal of SO$_4$ would increase as the bacterial population acclimatized to the increase in influent SO$_4$ concentration. The extent of SO$_4$ removal remained relatively constant over time with a slight decrease in column 1 (Tables 3 and 4). This observation suggests that the influent SO$_4$ concentration no longer limited the extent of sulfate reduction. Other factors that may limit the rate of sulfate reduction include the availability of nutrients prin-
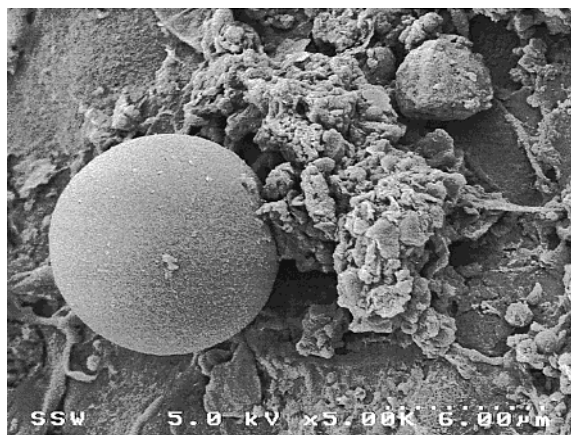

FIGURE 8. Representative SEM micrograph of spheroidal Fe and S solids present on reactive media at termination of column experiment.

TABLE 6. Organic Composition of Reactive Mixtures and Calculated Total Nitrogen, Phosphorus, and Carbon Content Expressed as Dry Weight (g) and Dry Weight Percent (wt %)

column	sewage sludge	leaf mulch	wood chips	sawdust	total N	total P	total C
1	39 g	75 g	30 g	40 g	1.5 g	0.42 g	63 g
	21%	41%	16%	22%	0.8%	0.23%	34.1%
2		77 g		77 g	1.4 g	0.21 g	64 g
		50%		50%	0.9%	0.14%	41.3%

cipally N and P, insufficient concentrations of labile C, inadequate retention times, or substrate limitations.

Concentrations of P, N, and C were determined on each organic substrate and calculated for each reactive mixture (Table 6), and concentrations of DOC, organic acids, o-PO$_4$, and NH$_4$ were determined on column effluent samples (Table 7). Results indicated that there was measurable C (in the form of propionic acid) and inorganic P (as o-PO$_4$), but inorganic N (as NH$_4$) was not detected, suggesting that inorganic N may have limited the rate of sulfate reduction. Previous batch studies (5) indicated that aqueous NH$_4$ was rapidly depleted in several of the mixtures tested. To determine whether the sulfate reduction rate was N limited, 7 mg/L of N as NH$_4$Cl was added to the influent at approximately 18.5 pv (feed 6). Rates of sulfate reduction remained relatively constant after NH$_4$Cl was added. It is unclear whether the addition of N (as NH$_4$Cl) was beneficial; more work is necessary. However, samples collected for δ^{34}S indicate greater enrichment factors after addition of NH$_4$Cl (Table 5). Inadequate retention times, substrate limitations, and lack of sites suitable for microbial attachment remain possible limitations to the rate of sulfate reduction.

Estimating the Longevity of the Carbon Source. The longevity of the carbon source was estimated by calculating the mass of C loss from the columns. It was assumed that the only C loss that occurred in the column was through leaching and direct consumption in the reduction of SO$_4$ to H$_2$S generalized by the following equation:

$$\text{SO}_4^{2-} + 2\text{CH}_2\text{O} \rightarrow \text{H}_2\text{S} + 2\text{HCO}_3^- \quad (9)$$
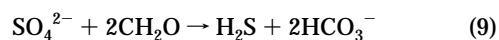
where 2 mol of C is oxidized for every mole of SO$_4$ reduced. Carbon loss due to the reduction of SO$_4$ was estimated based upon the amount of SO$_4$ reduced in each column. This mass of SO$_4$ reduced was applied to the reaction stoichiometry given above to estimate the mass of C consumed in the reduction of SO$_4$. The amount of C leached from the columns

TABLE 7. Column Effluent Data Showing Aqueous Concentrations of Phosphate (o-PO₄), Ammonium (NH₄), Dissolved Organic Carbon (DOC), and Volatile Fatty Acids (Organic Acids)[a]

sample	pv	DOC (mg/L)	acetic acid (mg/L)	propionic acid (mg/L)	butyric acid (mg/L)	formic acid (mg/L)	PO₄ (mg/L)	NH₄ (mg/L)
column 1	18	3.0	<5	36	<5	<1	9.8	na
column 1	22	6.5	na	na	na	na	8.15	<1
column 2	19	11.0	<5	340	<5	<1	1.9	na
column 2	22	8.0	na	na	na	na	0.80	<1

[a] pv = pore volume; na = not analyzed.

was estimated using measured effluent DOC averaged over the total volume passed through each column.

The total amount of SO_4 reduced for column 1 containing leaf mulch, sawdust, sewage sludge, and wood chips was 9.4 g (0.3 mol) and for column 2 containing leaf mulch and sawdust was 14.6 g (0.4 mol). These values were calculated based upon the difference between the measured effluent SO_4 concentrations considering sulfate reduction and conservative transport and the modeled effluent SO_4 concentration considering conservative transport only. The calculated mass of SO_4 reduced does not consider SO_4, which may have been released and subsequently reduced through the dissolution of gypsum. Thus, the calculated mass represents the minimum amount of SO_4 reduced.

Estimated values of C leached from the mixtures were 0.9 g (0.08 mol) for column 1 and 1.1 g (0.09 mol) for column 2. The amount of C available in each column was determined from analytical compositions of the organic substances (Table 6). Column 1 contained 63 g (5.3 mol) of C, and column 2 contained 64 g (5.3 mol) of C. On the basis of the stoichiometric reaction between organic C and SO_4 (eq 9), 2 mol of C is oxidized for each mole of SO_4 reduced. Therefore, combining the amount of C consumed through oxidation/reduction reactions and C leaching, a minimum of 0.1 mol of C (5.25% of the available C) was consumed in column 1 and a minimum 0.4 mol of C (7.5% of the available C) was consumed in column 2. The difference in C consumed between the columns is directly related to the amount of C oxidized through sulfate reduction reactions (0.1 mol vs 0.4 mol in columns 1 and 2, respectively) as the amounts of C leached from the columns were similar (0.08 mol in column 1 and 0.09 mol in column 2). Tables 3 and 4 show the calculated rates of SO_4 reduction: column 2 (leaf mulch and sawdust) averaged 200 mmol d^{-1} m^{-3} higher than column 1 (leaf mulch, sawdust, sewage sludge, and wood chips).

Studies by Eger and Wagner (16), using bioreactors containing organic mixtures (yard waste, horse manure, sawdust, and municipal compost) to enhance sulfate reduction, found that <5% of the C present was utilized before the system could no longer support SO_4 reduction. A decrease in the sulfate reduction rates with time was anticipated as the easily decomposable fraction of C was utilized. Both columns utilized >5% of the C available, and although the observed sulfate reduction rates decreased slightly in column 1, they remain high throughout the duration of the experiment. The increase in C utilization and the high sulfate reduction rates as compared to previous studies (16–18) are attributed to longer residence times and a higher input solution pH, the main differences between the studies.

The sulfate reduction rates determined from these experiments were used in the design of a full-scale reactive barrier at the Nickel Rim mine site (4). A comparison of the sulfate reduction rates observed in these experiments to those observed at Nickel Rim is presented by Benner et al. (23). At the field installation, the temperature and the groundwater velocity are more variable and uncertain than in the column experiments. After accounting for these variations, Benner et al. (23) concluded that the reaction rate observed in the

laboratory was approximately two times greater than in the field. This level of agreement is very good in consideration of the uncertainties associated with the field installation.

Literature Cited

(1) Dubrovsky, N. M.; Morin, K. A.; Cherry, J. A.; Smyth, D. J. A. *Water Pollut. Res. J. Can.* **1984**, *19*, 55–89.
(2) Morin, K. A.; Cherry, J. A.; Davé, N. K.; Lim, T. P.; Vivyurka, A. J. *J. Contam. Hydrol.* **1988**, *2*, 305–322.
(3) Blowes, D. W.; Ptacek, C. J. United States Patent 5,362,394, 1994.
(4) Benner, S. G.; Blowes, D. W.; Ptacek, C. J. *Ground Water Monit. Rem.* **1997**, *Fall*, 99–107.
(5) Waybrant, K. R.; Blowes, D. W.; Ptacek, C. J. *Environ. Sci. Technol.* **1998**, *32*, 1972–1979.
(6) Benner, S. G.; Blowes, D. W.; Gould, W. D.; Herbert, R. B., Jr.; Ptacek, C. J. *Environ. Sci. Technol.* **1999**, *33*, 2793–2799.
(7) Benner, S. G.; Gould, W. D.; Blowes D. W. *Chem. Geol.* **2000**, *169*, 435–448.
(8) Richards, F. A. In *Chemical Oceanography*; Riley, J. P., Skirrow, G., Eds.; Academic Press: New York, 1965; Vol. 1, pp 611–645.
(9) Reeburgh, W. S. *Annu. Rev. Earth. Planet. Sci.* **1983**, *11*, 269–298.
(10) Herbert, R. B., Jr.; Benner, S. G.; Blowes, D. W. *Appl. Geochem.* **2000**, *15*, 1331–1343.
(11) Nordstrom, D. K. *Geochim. Cosmochim. Acta* **1977**, *41*, 1835–1841.
(12) van Genuchten, M. Th.; Parker, J. L. *Determining Transport Parameters from Laboratory and Field Tracer Tests*; Virginia Agricultural Experiment Station Bulletin 84-3; 1984.
(13) Mills, A. L.; Bell, P. E.; Herlihy, A. T. In *Acid Stress and Aquatic Microbial Interactions*; Rao, S. S., Ed.; CRC Press: Boca Raton, FL, 1989; pp 1–19.
(14) Allison, J. D.; Brown, D. S.; Novo-Gradac, K. J. *MINTEQA2/PRODEFA2, A Geochemical Assessment Model for Environmental Systems: Version 3.0 User's Manual*; U.S. Environmental Protection Agency: Athens, GA, 1990; 106 pp.
(15) Ball, J. W.; Jenne, E. A.; Nordstrom, D. K. *Am. Chem. Soc. Symp. Ser.* **1979**, *No. 93*, 815–836.
(16) Eger, P.; Wagner, J. *Proceedings of Sudbury'95–Mining and the Environment*; CANMET: Ottawa, ON, 1995; Vol. 2, pp 515–524.
(17) Dvorak, D. H.; Hedin, R. S.; Edenborn, H. M.; McIntire, P. E. *Biotechnol. Bioeng.* **1992**, *40*, 609–616.
(18) McIntire, P. E.; Edenborn, H. M. *Proceedings of the Mining and Reclamation Conference and Exhibition*; West Virginia University: Morgantown, WV, 1990; Vol. 2, pp 409–416.
(19) Mills, A. L. *Soil Reclamation Processes*; Klein, D., Tate, R. L., Eds.; Marcel Dekker: New York, 1985; pp 35–81.
(20) Spiro, B.; Aizenstat, Z. *Nature (London)* **1977**, *269*, 235–237.
(21) Clark, I. D.; Fritz, P. *Environmental Isotopes in Hydrogeology*; Lewis Publishers: Boca Raton, FL, 1999.
(22) Nakai, N.; Jensen, M. L. *Geochim. Cosmochim. Acta* **1964**, *28*, 1893–1912.
(23) Benner, S. G.; Blowes, D. W.; Ptacek, C. J.; Mayer, K. U. *Appl. Geochem.* **2002**, *17*, 301–320.